Asymmetry of inner dynein arms and inter-doublet links in *Chlamydomonas* flagella

Khanh Huy Bui,[1] Hitoshi Sakakibara,[2] Tandis Movassagh,[1] Kazuhiro Oiwa,[2,3] and Takashi Ishikawa[1]

[1]Department of Biology, ETH Zurich, CH8093 Zurich, Switzerland
[2]Kobe Advanced Information and Communication Technology Research Center, National Institute of Information and Communications Technology, Kobe 651-2492, Japan
[3]Graduate School of Life Science, University of Hyogo, Hyogo 678-1297, Japan

Although the widely shared "9 + 2" structure of axonemes is thought to be highly symmetrical, axonemes show asymmetrical bending during planar and conical motion. In this study, using electron cryotomography and single particle averaging, we demonstrate an asymmetrical molecular arrangement of proteins binding to the nine microtubule doublets in *Chlamydomonas reinhardtii* flagella. The eight inner arm dynein heavy chains regulate and determine flagellar waveform. Among these, one heavy chain (dynein c) is missing on one microtubule doublet (this doublet also lacks the outer dynein arm), and another dynein heavy chain (dynein b or g) is missing on the adjacent doublet. Some dynein heavy chains either show an abnormal conformation or were replaced by other proteins, possibly minor dyneins. In addition to nexin, there are two additional linkages between specific pairs of doublets. Interestingly, all these exceptional arrangements take place on doublets on opposite sides of the axoneme, suggesting that the transverse functional asymmetry of the axoneme causes an in-plane bending motion.

Introduction

Most motile cilia and flagella possess the "9 + 2" structure in which nine microtubule doublets surround two central singlets. Although the canonical 9 + 2 structure looks symmetric, diverse waveforms are generated. For example, sperm displays symmetric waveforms, whereas a significant number of cilia, such as in the epithelial airway, beat asymmetrically. Particularly in the case of *Chlamydomonas reinhardtii*, the motion is highly asymmetric, as the effective and recovery strokes are distinctively different (Brokaw and Luck, 1983). Thus, there must be some degree of asymmetry in the axonemal structure. *C. reinhardtii* flagella have outer dynein arms (ODAs) on only eight out of nine doublets (Hoops and Witman, 1983). This asymmetry is not essential for asymmetrical bending; however, the *oda1* mutant, which completely lacks ODA, makes a normal bending motions (Kamiya and Okamoto, 1985). Other asymmetric characteristics are the 1-2 bridge, also called two-part bridge, between doublets 1 and 2 and the beaklike features on doublets 1, 5, and 6 (Witman et al., 1972; Hoops and Witman, 1983). In our previous work by cryo-electron tomography and single-particle averaging on wild-type and various *C. reinhardtii* mutants (Bui et al., 2008), the molecular architecture of the inner dynein arm (IDA) in vivo was presented; the six single-headed dynein heavy chains (dyneins a–e and g) are roughly collinear, whereas the heterodimer dynein f, also called I1, is at a closer distance to the A-tubule. However, the pattern of IDA among doublets was not explored because the structure was the total average of all doublets. Nevertheless, there was a hint of heterogeneity or flexibility in our structure in that the density of dynein b/g adjacent to radial spoke S1 was weaker compared with that of other inner arm dyneins.

Although dynein motors generate force to slide microtubules past each other, bending is believed to result from the inter-doublet link (IDL), known as nexin, connecting consecutive doublets (Gibbons, 1963; Summers and Gibbons, 1971; Brokaw, 1980; Hoops and Witman, 1983). Although not biochemically characterized, nexin is assumed to demonstrate elastic properties (Minoura et al., 1999) and is one of the most susceptible parts of the axoneme to elastase and trypsin digestion (Summers and Gibbons, 1971, 1973; Brokaw, 1980). To allow the doublet to slide a large distance, it was suggested that nexin can detach and reattach to the outer doublet microtubules (Bozkurt and Woolley,

Correspondence to Takashi Ishikawa: takashi.ishikawa@mol.biol.ethz.ch

Abbreviations used in this paper: DC, docking complex; DRC, dynein regulatory complex; IC, intermediate chain; IDA, inner dynein arm; IDL, inter-doublet link; LC, light chain; ODA, outer dynein arm; SNR, signal to noise ratio.

The Rockefeller University Press $30.00
J. Cell Biol. Vol. 186 No. 3 437–446
www.jcb.org/cgi/doi/10.1083/jcb.200903082

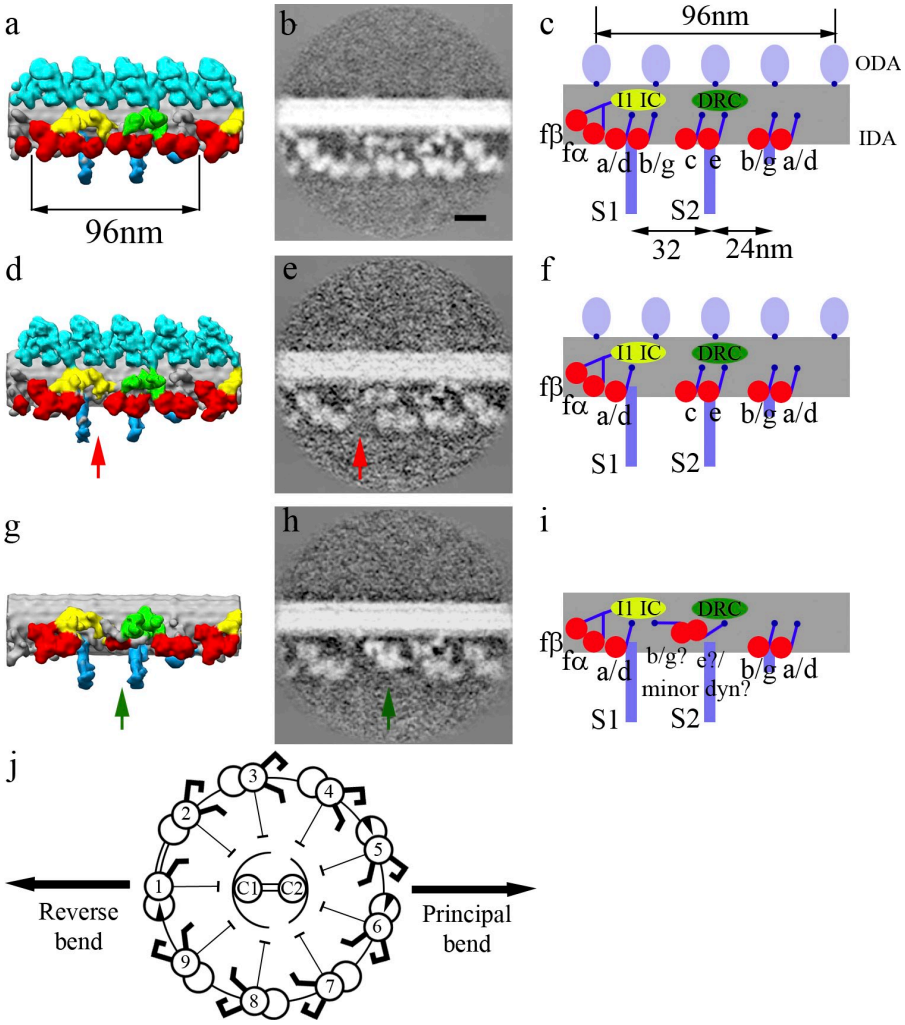

Figure 1. **The architecture of the IDAs on individual microtubule doublets.** (a, d, and g) The surface rendering of doublets 2–8 (a), 9 (d), and 1 (g). (b, c, e, f, h, and i) Same section across the averaged density map and the schematic representation of doublets 2–8 (b and c), 9 (e and f), and 1 (h and i) showing the inner arm dynein pattern. Red arrows show the position of the absent dynein b/g adjacent to radial spoke S1, and green arrows show the bulb density on doublet 1. Red, IDA; light blue, ODA; blue, radial spokes; green, DRC; yellow, light chain (LC)/IC of dynein f. The heads of radial spokes were also seen (not depicted) but have been trimmed in these figures to show only the area around the doublets. (j) The doublet-numbering order was performed as described by Hoops and Witman (1983), with doublets 1, 5, and 6 having the beaklike projection and a 1-2 bridge between doublets 1 and 2. Double-ended black arrows indicate the beating plane. Bar, 20 nm.

1993; Minoura et al., 1999). Nexin was structurally characterized by freeze-fracture deep-etch (Burgess et al., 1991; Bozkurt and Woolley, 1993) and cryoelectron microscopy (Nicastro et al., 2006) as a bifurcated structure repeating every 96 nm and emerging from near the dynein regulatory complex (DRC). In addition to nexin, there is a 1-2 bridge, connecting doublets 1 and 2 in some portions of the *C. reinhardtii* flagella (Hoops and Witman, 1983). However, structural characterization of the 1-2 bridge and its repeating pattern in the axoneme has yet to be performed. In this study, we exploited the technique of electron cryotomography and single-particle averaging and demonstrated asymmetrical features in the molecular organization and structure of each doublet in the axoneme 9 + 2 structure of *C. reinhardtii*. Although the pattern of the inner arm dyneins of doublets 2–8 are similar to our previously reported structure (Bui et al., 2008), dynein b/g adjacent to radial spoke S1 is lacking on doublet 9. Furthermore, the architecture of doublet 1 differs significantly from other doublets; dynein c is lacking, whereas dyneins e and b/g are either folded differently from those of doublets 2–8 or replaced by minor dyneins, suggesting functional diversity. In addition to the well-described bifurcated nexin link, two new inter-doublet linkages between particular doublets were found. From doublets 4, 5, and 9, there are linkages to the adjacent B-tubule emerging from near the intermediate chain (IC) of dynein f (I1). Another linkage emerges from the bulb density between radial spokes S1 and S2 on doublet 1 connecting to doublet 2. The 1-2 bridge (Hoops and Witman, 1983) between doublets 1 and 2 is surprisingly dense, with a periodicity of 8 nm. These highly asymmetric features of *C. reinhardtii* flagella could explain the planar waveform in forward swimming.

Results

By increasing the amount of data from electron cryotomograms of flagella from wild-type *C. reinhardtii* as well as those of mutants, we improved the signal to noise ratio (SNR) of averaged images of individual doublets and found that the molecular architecture of IDA depends on which of the microtubule doublets they were associated with. In addition, we also identified inter-doublet linkers between doublet pairs by examining round-shaped (uncompressed) flagella (see Materials and methods and Fig. S1 b).

Heterogeneity of molecular architecture of IDAs among doublets

We averaged the nine microtubule doublets from 28 flagella separately. The doublet without ODA was labeled doublet 1 after

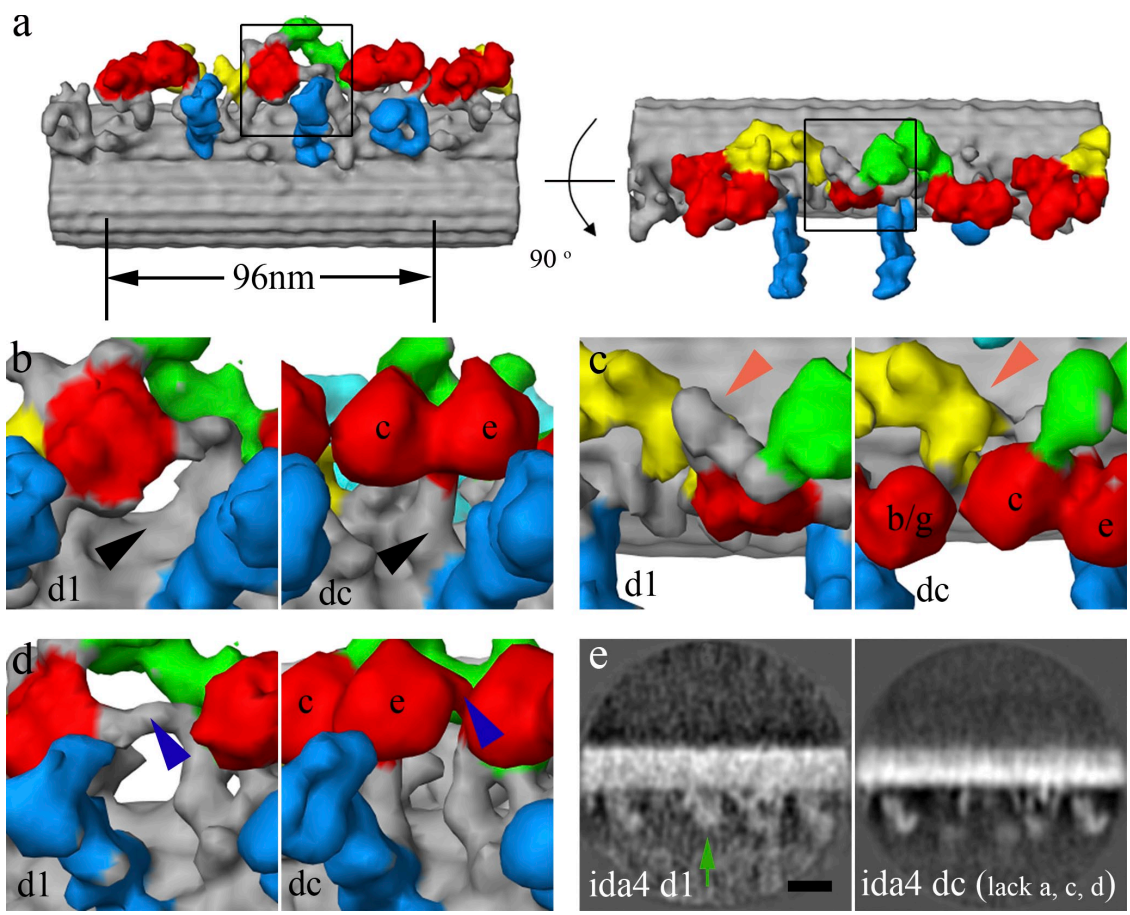

Figure 2. **Comparison of doublet 1 and the common IDA architecture.** (a) Overall view and 90° view. (b–d) Enlarged images of doublet 1 (boxed regions in a) shown at different viewing angles, with the common architecture (average doublets 2–8) used as a control on the right. Blue arrowheads, folded tail of dynein e; black arrowheads, positions where the dynein c tail should emerge (Bui et al., 2008) but is missing on doublet 1; orange arrowheads, additional density on doublet 1 behind dynein e. (e) Sections of the average of doublet 1 (d1; left) and doublets 2–8 (dc; right) of mutant *ida4*, showing that the lack of dynein c does not change the appearance of the bulb density on doublet 1. The green arrow shows the bulb density on doublet 1. Bar, 20 nm.

Hoops and Witman (1983; Fig. 1 j). Although ODA from doublets 2–9 are similar, the IDA arrangement on doublets 1 and 9 differs from the rest (Videos 1–3). The IDAs of doublets 2–8 possess the same molecular structure reported in our previous study (Bui et al., 2008), which we call the "common IDA architecture." The common IDA structure is also observed in the total average of all doublets from sea urchin sperm and *Tetrahymena thermophila* cilia (unpublished data). In the common structure, the six single-headed dynein rings are roughly colinear, and the N-terminal tails emerge from the distal end of all the dynein rings. Doublet 9 completely lacks dynein b/g adjacent to radial spoke S1 (Fig. 1, d and e, red arrows), although it retains the structure of all other inner arm dynein heavy chains. Notably, doublet 1 shows a distinctively different spatial arrangement of IDA (Fig. 1, g and h) from the common IDA architecture. The region between radial spokes S1 and S2 does not show the three single-headed dyneins b/g, c, and e found in other doublets but rather shows a bulb density much closer to the microtubule at 151 Å, measured from the surface of the A-tubule toward the end of the bulb density (Fig. 1, g and h, green arrows). In the common architecture, this distance is 226 Å from the A-tubule to the end of dynein e. This difference is consistent in all of the mutants analyzed in this paper (Table S1) and in our previous publication (Bui et al., 2008). In all individual structures of doublets 2–8, the density of both the ring and tail of dynein b/g adjacent to radial spoke S1 is weaker than that of the other dyneins (Fig. S1). This suggests that dynein b/g is either flexible or present at only partial occupancy along the flagellum. In all of the tomograms (wild type and mutants) having the 1-2 bridge (as described in "1-2 bridge between..."), we observed that doublet 5 consistently lacks dynein b/g adjacent to radial spoke S1. One possibility is that the composition of IDA differs in this dynein b/g also along the flagella. Another possible reason is that this dynein b/g is so weakly attached that it can easily be lost during the purification process.

Missing or differently folded inner arm dyneins on doublet 1

As mentioned in the previous section, the structure of doublet 1 is significantly different from that of the other doublets. Doublet 1 has a bulb density close to the microtubule doublet instead of the distinct density for dynein b/g, c, and e seen in the common IDA architecture. To improve the SNR and resolution of doublet 1, we averaged doublet 1 from the wild type and mutants (*oda1*, *oda11*, *oda4*, and *oda4s7)*, which are known to have normal IDA (total of 405 vs. 153 96-nm repeats from wild type), yielding

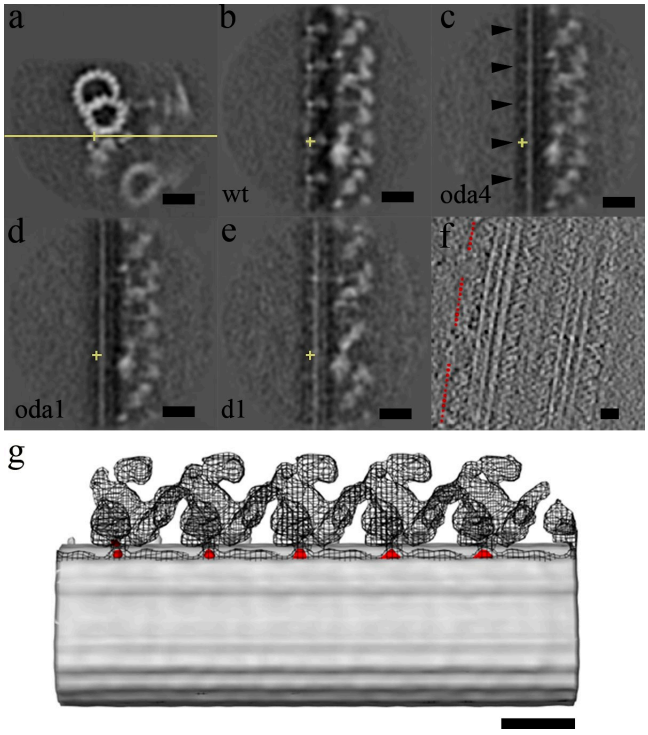

Figure 3. **DC analysis on wild type, *oda4* (lacking ODA but retaining DC), *oda1* (lacking both ODA and DC), and the doublet 1 average from wild type, *oda11*, *oda4*, and *oda4s7*.** The yellow crosses show the center of the extra density and are at the same position in all cross sections. (a) Cross section of the common IDA architecture of wild type with the yellow line indicating the plane of the yz section. (b) yz section of wild type (wt) showing the 24-nm repeat. (c) yz section of *oda4* also showing the 24-nm spacing (black arrowheads). (d) No 24-nm repeat is shown in *oda1*. (e) yz section of the doublet 1 average. (f) Horizontal section of a tomogram involving doublet 1 from wild-type flagellum. ODA is present but with no regular 24-nm periodicity. Red dotted lines indicate the regions with ODA. (g) Overlap of surface rendering of wild type, *oda4*, and the difference map between *oda4* and *oda1*, showing that the 24-nm periodicity from the difference map (red) is at exactly the same place as the interface of ODA with the A-tubule. The surface rendering of wild type and *oda4* are represented by mesh and gray surfaces, respectively. Bars, 20 nm.

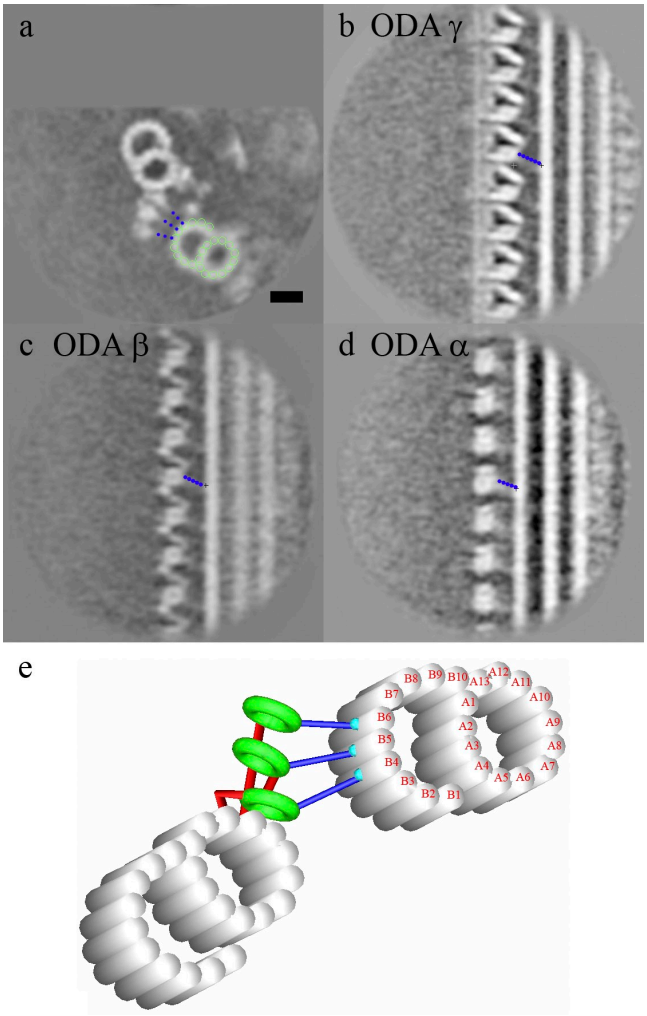

Figure 4. **The attachment of the ODA stalk to the adjacent microtubule.** (a–d) It is shown as a cross section (a), ODA γ (b), ODA β (c), and ODA α (d). The dotted blue lines indicate the stalk. The green circles indicate the protofilaments in the adjacent B-tubule. (e) A model of ODA stalk interaction with the adjacent B-tubule is shown. Bar, 20 nm.

better contrast and resolution for the structure of doublet 1. When compared with the common architecture, the disappearance of the tail of dynein c on doublet 1 (Fig. 2 b, black arrowheads) indicates that dynein c is completely absent in this doublet. This is consistent with the observation that the averaged map of doublet 1 from the *ida4* mutant, which lacks dyneins a, c, and d, still shows the bulb density similar to that of the wild type (Fig. 2 e). The bulb density is highly likely to be dynein because it has a tail-like structure emerging at the same place as the dynein e tail (Fig. 2 d, blue arrowheads) and a typical dynein doughnut-shaped projection (not depicted). The doublet 1 structure of *pf3* in the region of the 1-2 bridge (likely the proximal region; Hoops and Witman, 1983) shows that the bulb density is still present (Fig. S2). This implies that dynein e is replaced with another protein, likely one of the minor dyneins, which is localized at the proximal end (Yagi et al., 2009). Because >60% of our *pf3* data show a structure with the 1-2 bridge (as described in 1-2 bridge between doublets 1 and 2), which is supposed to be at the proximal region, *pf3* might be an exceptional mutant with most of the flagella having an architecture similar to that in the proximal region. Thus, it is not conclusive that a minor dynein also replaces dynein e from the 1-2 bridge region toward the tips. If dynein e is the bulb density, its tail is folded back (Fig. 2 d, blue arrowheads) and the head is positioned at the normal location of dynein c (Fig. 2 d, red density connecting to the dynein e tail). As the bulb density is still considerably larger than the dynein e head alone, dynein b/g might also be present, but stacked behind dynein e (Fig. 2 c, orange arrowheads). Alternatively, this extra density might come from IDL3, which is described in Additional linkage between doublets 1 and 2.

Abnormal ODAs and docking complexes (DCs) on doublet 1

We aligned and then compared the structures of the wild type, *oda4* (lacking ODA but retaining DC), and *oda1* (lacking both ODA and DC) and the averaged doublet 1 from wild type, *oda11*, *oda4*, and *oda4s7* in which the DC exists. In the wild type, at the interface between ODA and the A-tubule, there is a projection appearing with 24-nm periodicity (Fig. 3 b). When

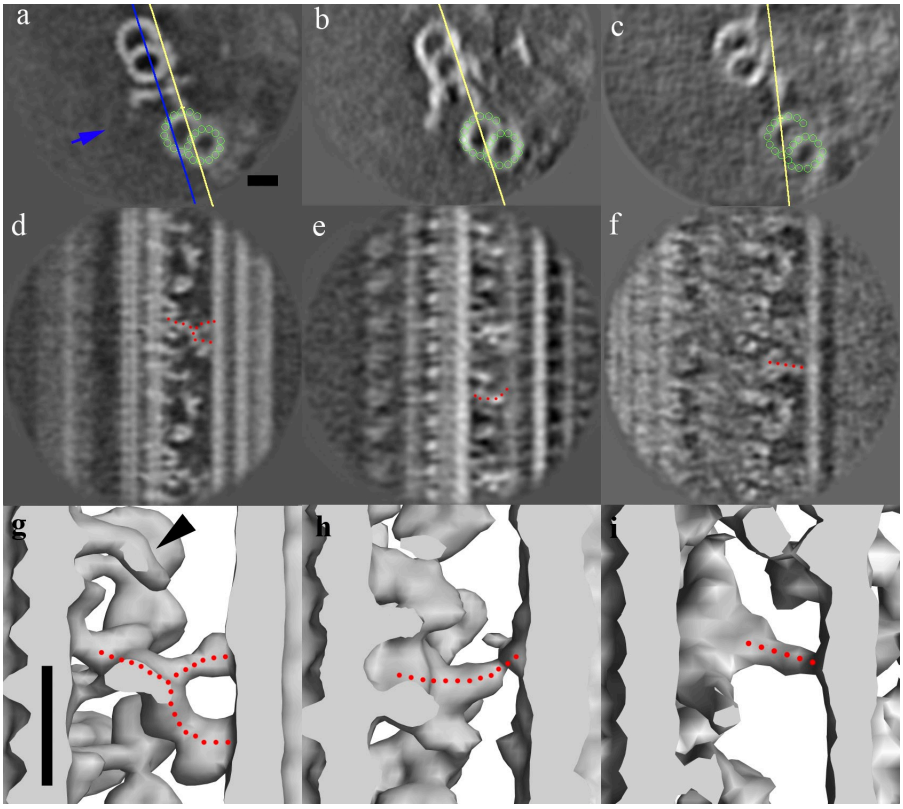

Figure 5. **The nexin linker, IDL2, and IDL3.** (a–i) Cross section and tilted views (yellow lines) and surface rendering, showing the circumferential nexin in all the doublets (a, d, and g), IDL2 from doublets 4, 5, and 9 (b, e, and h), and IDL3 from doublet 1 (c, f, and i). The green circles indicate the protofilaments in the adjacent B-tubule. The dotted red lines are drawn along the nexin, IDL2, and IDL3. The blue line and arrow in a indicate the cross section in the surface rendering (g–i) and the direction of view, respectively. The black arrowhead in g shows the protrusion above the radial spoke S3-like feature, which was identified as part of the nexin in our previous study (Bui et al., 2008), but it is now clear that it is not connecting to the nexin. Bars, 20 nm.

seen from the side, this density looks like a protrusion, as modeled by Wakabayashi et al. (2001; Fig. 3 g, red). In *oda4*, the intensity of this 24-nm repeating feature is still visible (although weaker than in the wild type; Fig. 3 c), but it completely disappears in *oda1* (Fig. 3 d). Thus, the 24-nm period projection is possibly a part of the DC. When overlapping the surface rendering of wild type and the difference map between *oda4* and *oda1*, the projections showed up exactly at the interface between ODA and the A-tubule (Fig. 3 g). In the averaged image of doublet 1 of wild type and all the mutants analyzed in this study, there is no projection with a regular spacing of 24 nm, implying that the DC is either completely lacking or incorrectly assembled on doublet 1 (Fig. 3 e). The presence of ODA on doublet as sparsely distributed clusters along doublet 1 in some of our datasets (Fig. 3 f and Table S2) suggests that ODA-DC is not completely missing on doublet 1.

ODA stalks between adjacent microtubule doublets

The stalks of ODA α, β, and γ heavy chains from the average of the round-shaped flagella are tilting toward the proximal end (Fig. 4). The orientations of these stalks are common among doublets 2–9, and they follow the regular array pattern of the ODA. The γ stalk connects to protofilament B4 (numbered according to Sui and Downing, 2006), whereas the β stalk links to protofilament B5 and the α stalk attaches to protofilament B6. Thus, each stalk seems to connect to a consecutive, specific protofilament on the B-tubule (Fig. 4, a and e). These features are common among all of the eight doublets, which retain ODA as arrays. We are unable to trace the stalks of IDAs in our structure.

Additional linkages on doublets 4, 5, and 9

All doublets possess the nexin structure as described in previous studies (Burgess et al., 1991; Bozkurt and Woolley, 1993; Nicastro et al., 2006). It is characterized as a bifurcated structure emerging near the DRC, connecting the A-tubule and the adjacent B-tubule with a 96-nm repeat (Fig. 5, a, d, and g). The Y-shaped head of the nexin is attached to protofilaments B2 and B3 of the adjacent B-tubule. We have found another linkage connecting doublets 4, 5, and 9 to doublets 5, 6, and 1, respectively (Fig. S3). To distinguish it from the circumferential nexin structure, we refer to it as IDL2. IDL2 also has a 96-nm periodicity and emerges near the IC of dynein f (Fig. 5, b, e, and h) with a slightly curved morphology (Fig. 5, b, e, and h), attaching to protofilaments B3 and B4 of the adjacent B-tubule. IDL2 connects to doublets 5, 6, and 1, which are the only doublets having the beaklike feature inside the B-tubule (Hoops and Witman, 1983). The beaklike projections on doublets 1, 5, and 6 appear to be a fiberlike structure running along the B5 and B6 protofilaments of adjacent B-tubules (Fig. 6). In terms of the morphology of flagella, IDL2 doubles the connections on the two opposite sites of the flagella (doublet groups 1-9 and 4-5-6).

Additional linkage between doublets 1 and 2

In addition to IDL2, we found another novel inter-doublet linkage, which we refer to as IDL3. Like the previously described 1-2 bridge (see Discussion; Witman et al., 1972; Hoops and Witman, 1983), the IDL3 interconnects doublets 1 and 2. The IDL3 emerges from the bulb density on doublet 1, which we speculate to be a minor dynein or dynein e, tilts

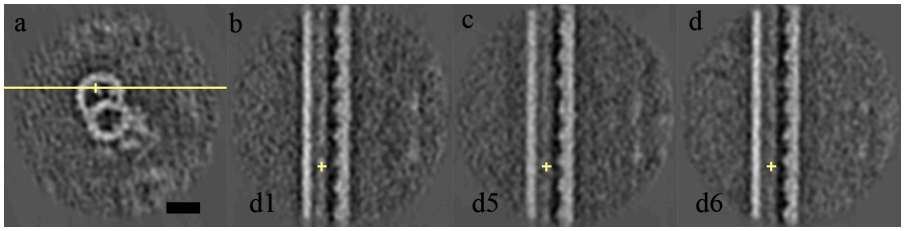

Figure 6. **The beaklike projections inside doublets.** (a) The vertical section shows the plane of view of the cross sections (yellow line). (b–d) Longitudinal sections of doublets 1 (b), 5 (c), and 6 (d). The yellow crosses in the yz cross sections show the beaklike feature and are at the same position as the yellow cross in a. Bar, 20 nm.

toward the proximal end, and connects to protofilaments B4 and B5 of the adjacent B-tubule (Fig. 5, c, f, and i). Because the density of IDL3 is strong, it is unlikely to be the stalk of dynein e or a minor dynein. Both IDL2 and IDL3 are localized only at the two strongly connected opposite sides (4-5-6 and 9-1-2).

1-2 bridge between doublets 1 and 2

In our data, only six out of 28 flagella had the 1-2 bridge, which was described previously (Witman et al., 1972; Hoops and Witman, 1983). It is remarkable that the 1-2 bridge has 8-nm periodicity, forming a surprisingly dense lattice (Fig. 7, a–c). Both links in the 1-2 bridge are straight, connecting the A-tubule with the adjacent B-tubule. The inside link is discontinuous at the DRC (Fig. 7 b, black arrowhead) and then appears again with same 8-nm periodicity. In addition to the 1-2 bridge with an 8-nm periodicity, another two linkages (Fig. 7, d and e) were also seen. The first linkage emerged at approximately the same position as the nexin, but it is straighter. The other linkage, ∼24-nm proximal to the first one, appears to be IDL3, as it has the same emergence point and morphology. Apparently, the first link replaces nexin in this proximal region while the IDL3 still exists. The architecture of IDA of doublet 1 in the presence of the 1-2 bridge is slightly different from the rest of doublet 1, whereas there is no significant difference in the bulb density between radial spokes S1 and S2 and dyneins b/g and a/d adjacent to S3; the region containing dynein f and a/d adjacent to S1 is different from the corresponding area without the 1-2 bridge (Fig. 7 f, blue arrowhead). This indicates that there is also heterogeneity along doublet 1. The differences among the nine doublets are summarized in Table S3.

Discussion

Our previous study (Bui et al., 2008) demonstrated that the architecture of IDA in situ in *C. reinhardtii* consists of one double-headed and six single-headed dynein heavy chains. In this study, our detailed analysis indicates that the common architecture is present in doublets 2–8 but differs from that of doublets 1 and 9 (Fig. 1, c, f, and i). Although doublet 9 has a slightly different IDA structure, it is expected that the sliding activity of doublet 9 is similar to other doublets; doublet 9 still has the normal ODA array, and the missing dynein (b/g beside spoke S1) does not have a significant microtubule-translocating velocity compared with other inner arm dyneins (Kagami and Kamiya, 1992). However, the dissimilarity in doublet 1 could make a significant difference.

Morphology of doublet 1 suggests a functional difference

Doublet 1 of *C. reinhardtii* lacks ODA (Huang et al., 1979; Hoops and Witman, 1983), which normally contributes two-thirds of the force generation (Kamiya, 1995). As shown in Fig. 3, the arrangement of ODA DC is abnormal on doublet 1. It is not completely missing, as seen in the mutant *oda1*, but might be incorrectly assembled, as we occasionally observed a sparsely distributed ODA on doublet 1 (Fig. 3 f; Huang et al., 1979; Hoops and Witman, 1983). Our study showed that both ODA and IDA of doublet 1 are significantly different from the common architecture; our comparative analysis showed that dynein c is absent on doublet 1. As dynein c is the fastest microtubule-translocating inner arm dynein (Kagami and Kamiya, 1992) and the important motor in high viscosity conditions (Yagi et al., 2005), the dynein-driven sliding activity between doublets 1 and 2 would be significantly slower than that of other pairs of microtubule doublets. In fact, the velocity of the double-mutant *ida9oda1* (lacking ODA and dynein c) is less than half that of *oda1* (lacking ODA) and one seventh of that of wild type (Yagi et al., 2005). If the bulb density on doublet 1 is dynein e (and also dynein b/g adjacent to radial spoke S1), these dyneins should fold differently from those on other doublets, with the tail of dynein e greatly extended compared with its usual conformation (Fig. 2 d) and the heads being much closer to the A-tubule than normal (151 Å compared with 226 Å normally). If the bulb density is a minor dynein replacing dynein e, it is the head of this substitute dynein that is significantly closer to the A-tubule than the normal dynein head in the common architecture. With either possibility, this would lead to the different outcome of the power stroke compared with normal IDA. For the remaining dyneins on the 96-nm unit, dynein f is reported to either not translocate microtubules (Kagami and Kamiya, 1992) or translocate microtubules tremendously slowly in vitro (Kotani et al., 2007), whereas dyneins a, d, and b/g are not as powerful motors as dynein c (Kagami and Kamiya, 1992). Thus, the sliding activity between doublets 1 and 2 will be markedly different, presumably reduced compared with other pairs of doublets. Furthermore, there is no mutant found yet that lacks dyneins c, e, and b/g, possibly because that combination of inner arm dyneins is essential for motility and gives doublet 1 a functionally unique role. This might be a particular characteristic of *C. reinhardtii* to allow its distinctive asymmetric waveform. In contrast to *C. reinhardtii*, sea urchin sperm has the symmetric snakelike waveform in spite of having a similar common IDA architecture (unpublished data). In addition to the heterogeneity of IDA architectures among doublets, inner arm dyneins are also reported to be heterogeneous along each individual doublet in *C. reinhardtii* (Piperno

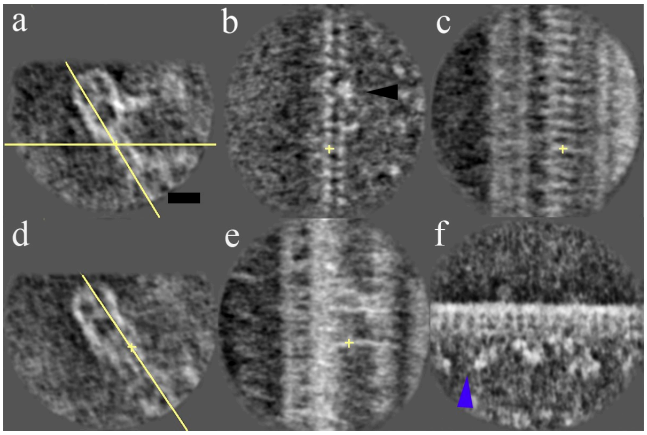

Figure 7. **Linkage between doublets 1 and 2 when the 1-2 bridge is present in a cross section.** (a, c, and e) The 1-2 bridge (8-nm period) in the xy plane (a), xz plane (c), and tilted section along the linkage (e). (b and d) The other two dominant linkages in the cross section (b) and tilted section along the two dominant linkages (d) are shown. The yellow crosses in b and c and e indicate the same position as the yellow crosses in a and d, respectively. Yellow lines in a and d indicate the planes of sections in b and c and e, respectively. The black arrowhead in b indicates the region where the inner bridge is discontinued. (f) Longitudinal section showing IDA of wild-type doublet 1 in the region of the 1-2 bridge. The blue arrowhead points to the difference from doublet 1 structure outside the 1-2 bridge region (Fig. 1 h). Bar, 20 nm.

and Ramanis, 1991). The minor species of inner arm dyneins DHC3, DHC4, and DHC11 are found to be localized exclusively to the proximal end, where they might replace the normal dyneins (a–g) for waveform optimization and other functions (Yagi et al., 2009). In our analysis of wild type and *pf3* mutant (Fig. S2), dynein e is highly likely to be replaced by minor dynein at the proximal portion of the flagella (1-2 bridge region). No structural difference was found on doublets 2–9 between the proximal portion of the flagella (region with 1-2 bridges) and other regions. Thus, even if there is a replacement by minor inner arm dyneins, the overall structure in the 96-nm repeat does not appear to be changed. The asymmetry of dynein arms (ODA and IDA) among doublets raises the question of how dynein architectures differentiate among doublets. Our analysis of the ODA DC gives a partial answer to that question: the inability to assemble the docking structure correctly causes the disappearance of the associated dyneins, but why the docking structure assembles differently remains unknown. Other proteins might bind on the inside of the microtubule and provide protofilament-specific anchoring sites for the DC, but we have not observed any such structure inside the lumen of the B-tubule that is missing only on doublet 1. How minor dynein replaces dynein e only on doublet 1 or why dynein e and probably dynein b/g fold differently on doublet 1 are unanswered questions as well. The lack of dynein c is not responsible for the different folding because the *ida9* mutant, which lacks dynein c, still shows the common architecture of IDA in other doublets (Bui et al., 2008).

Asymmetric connections between adjacent doublets

Nexin, the circumferential link that was first recognized by Gibbons (1963), is believed to convert the sliding into a bending motion in axonemes, as in flagella treated with elastase or trypsin, only sliding disintegration of microtubule doublets was reported (Summers and Gibbons, 1971; Brokaw, 1980). We found that nexin links with a bifurcated structure that was similarly shown in previous studies (Burgess et al., 1991; Bozkurt and Woolley, 1993; Nicastro et al., 2006) between all adjacent pairs of microtubule doublets. The nexin link emerges from the DRC and connects to protofilaments B2 and B3 of the adjacent microtubule doublet. The attachment point on the B-tubule is similar to that for nexin in sea urchin sperm reported by Sui and Downing (2006), which is between protofilaments A9–11 and the adjacent protofilament B2. In the presence of DRC, as in our structure, the nexin appears to emerge from the DRC but not directly from protofilaments A9–11 as in the naked sea urchin sperm axoneme doublet (Sui and Downing, 2006). It is possible that the nexin is a part of the DRC. In our previous publication (Bui et al., 2008), we suggested that the protrusion above the feature resembling the radial spoke S3 (Fig. 1 a and Fig. 5 g) might be nexin. Now we see that this is not the case, as it does not reach the B-microtubule (Fig. 5 g, black arrowhead). We have identified one inter-doublet linkage (IDL2) from doublets 9, 4, and 5 to doublets 1, 5, and 6, which contain the beaklike features (Fig. 6), and another (IDL3) between doublets 1 and 2. The binding of the beaklike features to protofilaments B5 and B6 might cause structural changes in the protofilaments, facilitating the binding of IDL2 to protofilament B3. With a higher resolution study such as that by Sui and Downing (2006), it might be possible to clarify the relationship between IDL2 and the beaklike features. In longitudinal sections, the beaklike feature reveals itself as a fiberlike structure (Fig. 6). It might be one of the inner microtubule–associated proteins, such as tektin, which function in stabilizing the microtubule doublet (Sui and Downing, 2006) and possibly serve as anchor points for IDL2. The other linkage (IDL3) emerges from the bulb density on doublet 1 and connects to doublet 2. IDL2 and IDL3 could reinforce the connections on opposite sides of the flagellum (doublet groups 9-1-2 and 4-5-6). With two linkages per 96 nm, the two sides will presumably be more rigid and have less inter-doublet sliding motion than the rest of the microtubule doublets. As shown in Fig. 8, doublets 9-1-2 of one flagellum face doublets 9-1-2 of the other, whereas doublets 4, 5, and 6 are on the outside of the pair (Hoops and Witman, 1983). During swimming, doublets 1 and 9 are on the convex surface of the principal bend of the effective stroke, whereas doublets 4, 5, and 6 are on the opposite side (Mitchell, 2003). The property of strongly connected doublets on opposite sides of the flagellum in *C. reinhardtii* is an important factor in restraining the flagellum to move back and forth in a plane instead of 3D helical or conical motion with all the doublet pairs equally connected.

The dense 1-2 bridge between doublets 1 and 2

The 1-2 bridge only appears between doublets 1 and 2 and seems to be a specialized feature in *C. reinhardtii*. The study by Hoops and Witman (1983), based on electron microscopy of plastic-embedded sections, suggested that the 1-2 bridge exists only in the proximal quarter of the flagella. That observation is indirectly supported by our data; only 6 out of 28 flagellar

fragments show the 1-2 bridge. To date, the 1-2 bridge has never been characterized in a longitudinal orientation showing its repeating pattern or morphology. Our analysis proved that the 1-2 bridge has an 8-nm periodicity. Compared with the circumferential nexin, the connections on the 1-2 bridge are 24 times more dense (2 × 12 connections per 96 nm). The density of the 1-2 bridge apparently increases the rigidity between doublets 1 and 2 considerably in the proximal quarter of the flagellum. In addition to the 1-2 bridge, IDL3 and the other inter-doublet linkage (Fig. 7, d and e) also contribute to the rigidity of doublet pair 1-2. As a result, the sliding activity between doublets 1 and 2 should be minimal at the basal region of the flagella. Together with IDL2 and IDL3, the 1-2 bridge reinforces the two opposite side groups (doublets 9-1-2 and 4-5-6), which could make the waveform planar. Another possible reason for the densely packed 1-2 bridges is that by making the flagella so rigid at the proximal end, it will form a principal bend with a large radius of curvature, which can contribute to the asymmetric waveform of *C. reinhardtii*. The asymmetric linkage is also observed in other organisms. In sea urchin sperm, there is a bridge between doublets 5-6 (different doublet numbering system) distinct from other doublet pairs (Afzelius, 1959). This 5-6 bridge is equivalent to the 1-2 bridge in *C. reinhardtii*, as it is in the plane of and on the outside of the principal bend (Sale, 1986; Mitchell, 2003). In sliding disintegration, which is the disruption of axonemes into two subsets of microtubules by (active) sliding, with one set (the thick bundle) consisting of five and the other of four doublets, the dominant pattern of the thick bundle is 8–3, i.e., consisting of doublets 8–3 (nonelastase-treated axoneme; Sale, 1986; Mitchell, 2003), which is equivalent to 8–4 in *C. reinhardtii's* doublet-numbering definition. This sliding disintegration pattern is consistent with our observation of the inter-doublet linkage pattern. The axoneme separates between doublet pairs 8-9 and 3-4 where there is only the nexin present but not at the pairs where other IDLs are present (IDL2, IDL3, and the 1-2 bridge). The 1-2 bridge region of the flagella has some special features compared with other regions. Apart from the 1-2 bridge, the inter-doublet linkage from near the DRC of doublet 1 is different from that of nexin. In addition, there is a slight difference in IDA architecture of doublet 1 adjacent to radial spoke S1 (Fig. S2, arrowheads). Dynein b/g adjacent to radial spoke S1 is also absent from doublet 5 in this region (unpublished data). The 1-2 bridge is located at the proximal end of the flagella (Hoops and Witman, 1983) where dynein b (DHC5) is found to be absent or present only in a very low amount (Yagi et al., 2009). The authors also speculated that the minor species of inner arm dynein DHC4 in the proximal ∼2-µm portion might replace dynein b (DHC5). The lower density of dynein b/g in our doublet 5 map could be explained as a result of partial occupancy and asymmetric replacement; doublet 5 might be exceptional and lack minor dynein. Although the position of dynein b/g is occupied by minor dynein in other doublets, that position on doublet 5 could be empty. As seen in this study, heterogeneity along one microtubule doublet between proximal and distal parts will be an important topic in the future. Currently, the limitation of the size of the camera prohibits us to analyze the whole flagella simultaneously. With our current data acquisition setup, a tomogram only contains an ∼1.5-µm length of the flagella, whereas the length of the whole flagellum is normally between 10 and 15 µm.

ODA stalks attaching at consecutive protofilaments

The ODA stalks are all tilted toward the proximal (basal) end of the flagella. In addition, the ODA stalks (γ, β, and α) attach to the adjacent B-tubule at consecutive protofilaments (B4, B5, and B6).The binding of ODA stalks to the specific protofilaments is probably because of the fact that tubulins of the individual protofilaments might undergo different posttranslational modification (Gaertig and Wloga, 2008), so they bind to specific microtubule-associated proteins on the surface. Another simple explanation would be that the geometric distance limits the binding of stalk heads to a specific protofilament on the adjacent B-tubule. High resolution structural studies of reconstructed dynein–microtubule complexes (Oda et al., 2007) will allow this question to be clarified.

Asymmetric waveform of *C. reinhardtii* as the result of asymmetric flagellar structure

As described in the previous sections, all the asymmetry among the nine microtubule doublets in the 9 + 2 axoneme in *C. reinhardtii* flagella is found on doublets 4-5-6 and 9-1-2, which are located on the opposite sides of the axoneme. The strongly connected strips on opposite sides of the flagella function to keep flagellar beating in the plane joining the two stiffened strips. Furthermore, if one side generates stronger power strokes, it can induce an asymmetric bending motion, which is not possible from symmetric power strokes among nine microtubule doublets (Fig. 8). The rigidity at the basal part of the flagella created by the dense 1-2 bridge can also help form the large curvature of the principal bend. According to the switching-point hypothesis proposed by Satir (1989), only half of the doublets are active at any one time, and a switch of activity alternates between the halves. Our result of distinct strong (4-5-6) and weak (9-1-2) sides in the *C. reinhardtii* flagellum agrees with this hypothesis. Thus, each side (strong and weak) forms a distinct functional unit that alternates between the two halves, thereby creating the asymmetric, planar waveform. This interpretation, based on our structure, is not enough to explain symmetric backward swimming with high calcium concentrations (Bessen et al., 1980). In backward swimming, the different mechanism of regulation of activity of specific doublets by calcium concentration through the central pair and radial spoke system might balance out the force generation between the two sides to compensate for the asymmetry in structure. The central pair, which is structurally and biochemically asymmetric (Adams et al., 1981; Goodenough and Heuser, 1985), can also play a role in the asymmetric bending motion of the flagella. The central pair is believed to transmit signals to the dynein arms through the radial spoke, regulating the active doublets. The asymmetry of the central apparatus is thought to define the location of active microtubule sliding (Wargo and Smith, 2003). Studies in sea urchin sperm (Bannai et al., 2000; Nakano et al., 2003; Yoshimura et al., 2007)

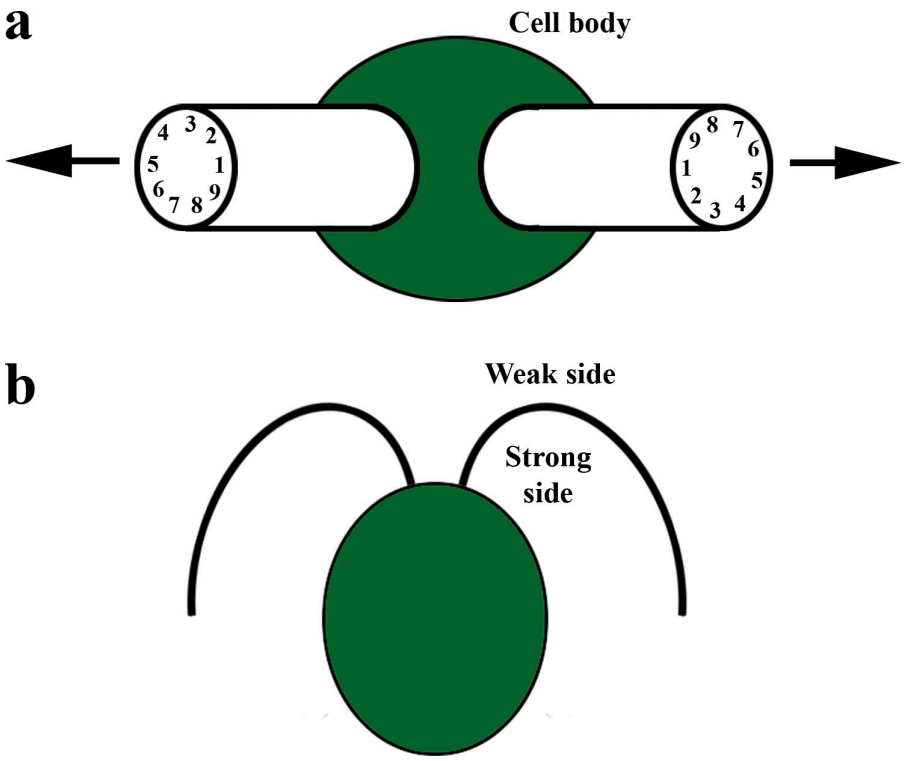

Figure 8. **Hypothesis of the mechanism of planar asymmetrical bending motion of flagella.** (a) Doublet order of flagella at the basal body of *C. reinhardtii* (Hoops and Witman, 1983), showing that doublets 1 of the two flagella are facing each other. Arrows indicate the plane of bend. (b) Illustration of the generation of planar asymmetric waveform by strong and weak sides is shown.

showed that at high ATP concentration, the presence of the central pair–radial spoke system is essential for waveform regulation, whereas it is not essential at low ATP concentration. At low ATP concentration, the asymmetric structures of IDA, ODA, and inter-doublet linkage are required for the asymmetric bending. As we have shown in this study, the ODA and IDA of microtubule doublets in *C. reinhardtii* can deviate from the common architecture, and this asymmetry may induce the specialized waveform. It will be very interesting to look for specialized structural deviations of the molecular architecture of axonemes from further organisms.

Materials and methods

Cell culture and flagella purification

In this study, some of the data from *C. reinhardtii* 137c wild-type, *oda11*, and *oda4s7* mutants were obtained from our previous studies (Ishikawa et al., 2007; Bui et al., 2008). Additionally, *oda1* and *oda4* mutants were used (Table S1). Wild-type and mutant strains were cultured in Tris-Acetate-Phosphate medium (Gorman and Levine, 1965). The dibucaine method (Witman, 1986) was used to isolate the axonemes. The intact axonemes were centrifuged down at 5,200 *g* for 20 min at 4°C, demembraned with 30 mM Hepes, pH 7.4, 5 mM $MgSO_4$, 1 mM DTT, 0.5 mM EDTA, 25 mM KCl, 0.5% (wt/vol) polyethylene glycol (20,000 molecular weight), and 0.8% NP-40, and centrifuged down again at 5,200 *g* for 20 min at 4°C after which the pellet containing the flagella was resuspended in 30 mM Hepes, pH 7.4, 5 mM $MgSO_4$, 1 mM DTT, 0.5 mM EDTA, 25 mM KCl, 0.5% (wt/vol) polyethylene glycol (20,000 molecular weight), and stored at 0°C for at least 1 d to ensure that no ATP was left in the solution before freezing.

Quick freezing and electron cryotomography

The specimen was frozen with liquid ethane at liquid nitrogen temperature using the Vitrobot (FEI). Images were collected as described previously (Ishikawa et al., 2007; Bui et al., 2008) using a transmission electron microscope (Tecnai F20; FEI) equipped with a field emission gun, an energy filter (GIF Tridiem; Gatan), and a 2,048 × 2,048 charge-coupled device camera (Gatan) at the accelerating voltage of 200 kV, a magnification of 19,303×, and an under focus of ∼2–4 µm. Tomographic images from 60° to 60° were acquired by Explore3D (FEI). To select perfectly round-shaped flagella without compression (flattening) in ice, we carefully chose images having a diameter of 220 nm and later screened in 3D (Fig. S1 b) as we previously described (Bui et al., 2008).

Image analysis

The image analysis method to obtain the 96-nm average from the tomogram was similar to that of our previous study (Bui et al., 2008). In brief, tomograms were reconstructed by IMOD (Mastronarde, 1997) with fiducial marker alignment and R-weighted back projection. Subtomograms with pixel dimensions of 200 × 200 × 200 were boxed out with a roughly 96-nm period from the original tomogram by Bsoft (Heymann, 2001) and aligned along the microtubule by SPIDER (Frank et al., 1996) followed by inter-microtubule alignment. The identification of doublet number according to Hoops and Witman (1983) was based on features such as the beak-like projections on doublets 1, 5, and 6, 1-2 bridges between doublets 1 and 2, and the absence of ODA on doublet 1. Subaverages from doublets 1–9 of all tomograms were summed together to obtain the final average for each doublet. Averages were always deconvoluted by the total contribution of the missing wedge to keep data sampling isotropic as we described in our previous study (Bui et al., 2008). Surface rendering was performed by Chimera (Pettersen et al., 2004) after masking, denoising by a band-pass filter, and contrast inversion. Microtubule doublet (Figs. 5 and 7) and ODA stalk interaction (Fig. 4 e) models were drawn in IMOD (Kremer et al., 1996) by tracing the density map on the total average and transformed to fit the adjacent B-tubule. For the average of doublet 1, we added all the aligned doublet 1 averages from wild-type, *oda11*, *oda4s7*, *oda1*, and *oda4*, which all have normal IDA, to get a better SNR and higher resolution structure (total of 405 vs. 153 96-nm repeats from wild type). The IDA architectures among those mutants were also checked to ensure that they were similar. To calculate the difference map between *oda4* and *oda1*, the two density maps were aligned, least-square fitted within a mask to determine the correct intensity scale factor, and the scaled *oda1* map was subtracted from the *oda4* map.

Online supplemental material

Fig. S1 contains the longitudinal cross section of the average of each individual doublet (1–9) as well as the transverse cross section of the whole axoneme. Fig. S2 shows the cross section showing the IDA architecture of *oda11* and *pf3* in the 1-2 bridge region. Fig. S3 shows IDL2 in vertical sections of doublets 4, 5, and 9. Videos 1, 2, and 3 show the

surface rendering of the averaged volume of doublets 2–8, 9, and 1, respectively. Online supplemental material is available at http://www.jcb.org/cgi/content/full/jcb.200903082/DC1.

We thank Professor T.J. Richmond for the biochemical facility, Dr. David Sargent for critical reading of the manuscript, Dr. H. Gross and Peter Tittmann in the Electron Microscopy Center of ETH Zurich for technical support, and Professor R. Kamiya (University of Tokyo, Tokyo, Japan) for insightful discussion. This work was funded by grants from the Swiss National Science Foundation and National Centers of Competence in Research Structural Biology (NF 3100A0-107540 to T. Ishikawa), the Special Coordination Funds for Promoting Science and Technology (16083207 to K. Oiwa), and the Grant-in-Aid for Scientific Research on the Priority Area "Regulation of Nano-systems in Cells" by the Ministry of Education, Culture, Sports, Science and Technology (to K. Oiwa).

Submitted: 16 March 2009
Accepted: 13 July 2009

References

Adams, G.M., B. Huang, G. Piperno, and D.J. Luck. 1981. Central-pair microtubular complex of *Chlamydomonas* flagella: polypeptide composition as revealed by analysis of mutants. *J. Cell Biol.* 91:69–76.

Afzelius, B. 1959. Electron microscopy of the sperm tail; results obtained with a new fixative. *J. Biophys. Biochem. Cytol.* 5:269–278.

Bannai, H., M. Yoshimura, K. Takahashi, and C. Shingyoji. 2000. Calcium regulation of microtubule sliding in reactivated sea urchin sperm flagella. *J. Cell Sci.* 113:831–839.

Bessen, M., R.B. Fay, and G.B. Witman. 1980. Calcium control of waveform in isolated flagellar axonemes of *Chlamydomonas*. *J. Cell Biol.* 86:446–455.

Bozkurt, H.H., and D.M. Woolley. 1993. Morphology of nexin links in relation to interdoublet sliding in the sperm flagellum. *Cell Motil. Cytoskeleton.* 24:109–118.

Brokaw, C.J. 1980. Elastase digestion of demembranated sperm flagella. *Science.* 207:1365–1367.

Brokaw, C.J., and D.J. Luck. 1983. Bending patterns of *chlamydomonas* flagella I. Wild-type bending patterns. *Cell Motil.* 3:131–150.

Bui, K.H., H. Sakakibara, T. Movassagh, K. Oiwa, and T. Ishikawa. 2008. Molecular architecture of inner dynein arms in situ in *Chlamydomonas reinhardtii* flagella. *J. Cell Biol.* 183:923–932.

Burgess, S.A., D.A. Carter, S.D. Dover, and D.M. Woolley. 1991. The inner dynein arm complex: compatible images from freeze-etch and thin section methods of microscopy. *J. Cell Sci.* 100:319–328.

Frank, J., M. Radermacher, P. Penczek, J. Zhu, Y. Li, M. Ladjadj, and A. Leith. 1996. SPIDER and WEB: processing and visualization of images in 3D electron microscopy and related fields. *J. Struct. Biol.* 116:190–199.

Gaertig, J., and D. Wloga. 2008. Ciliary tubulin and its post-translational modifications. *Curr. Top. Dev. Biol.* 85:83–113.

Gibbons, I.R. 1963. Studies on the protein components of cilia from *Tetrahymena pyriformis*. *Proc. Natl. Acad. Sci. USA.* 50:1002–1010.

Goodenough, U.W., and J.E. Heuser. 1985. Substructure of inner dynein arms, radial spokes, and the central pair/projection complex of cilia and flagella. *J. Cell Biol.* 100:2008–2018.

Gorman, D.S., and R.P. Levine. 1965. Cytochrome f and plastocyanin: their sequence in the photosynthetic electron transport chain of *Chlamydomonas reinhardi*. *Proc. Natl. Acad. Sci. USA.* 54:1665–1669.

Heymann, J.B. 2001. Bsoft: image and molecular processing in electron microscopy. *J. Struct. Biol.* 133:156–169.

Hoops, H.J., and G.B. Witman. 1983. Outer doublet heterogeneity reveals structural polarity related to beat direction in *Chlamydomonas* flagella. *J. Cell Biol.* 97:902–908.

Huang, B., G. Piperno, and D.J. Luck. 1979. Paralyzed flagella mutants of *Chlamydomonas reinhardtii*. Defective for axonemal doublet microtubule arms. *J. Biol. Chem.* 254:3091–3099.

Ishikawa, T., H. Sakakibara, and K. Oiwa. 2007. The architecture of outer dynein arms in situ. *J. Mol. Biol.* 368:1249–1258.

Kagami, O., and R. Kamiya. 1992. Translocation and rotation of microtubules caused by multiple species of *Chlamydomonas* inner-arm dynein. *J. Cell Sci.* 103:653–664.

Kamiya, R. 1995. Exploring the function of inner and outer dynein arms with *Chlamydomonas* mutants. *Cell Motil. Cytoskeleton.* 32:98–102.

Kamiya, R., and M. Okamoto. 1985. A mutant of *Chlamydomonas reinhardtii* that lacks the flagellar outer dynein arm but can swim. *J. Cell Sci.* 74:181–191.

Kotani, N., H. Sakakibara, S.A. Burgess, H. Kojima, and K. Oiwa. 2007. Mechanical properties of inner-arm dynein-f (dynein I1) studied with in vitro motility assays. *Biophys. J.* 93:886–894.

Kremer, J.R., D.N. Mastronarde, and J.R. McIntosh. 1996. Computer visualization of three-dimensional image data using IMOD. *J. Struct. Biol.* 116:71–76.

Mastronarde, D.N. 1997. Dual-axis tomography: an approach with alignment methods that preserve resolution. *J. Struct. Biol.* 120:343–352.

Minoura, I., T. Yagi, and R. Kamiya. 1999. Direct measurement of inter-doublet elasticity in flagellar axonemes. *Cell Struct. Funct.* 24:27–33.

Mitchell, D.R. 2003. Orientation of the central pair complex during flagellar bend formation in *Chlamydomonas*. *Cell Motil. Cytoskeleton.* 56:120–129.

Nakano, I., T. Kobayashi, M. Yoshimura, and C. Shingyoji. 2003. Central-pair-linked regulation of microtubule sliding by calcium in flagellar axonemes. *J. Cell Sci.* 116:1627–1636.

Nicastro, D., C. Schwartz, J. Pierson, R. Gaudette, M.E. Porter, and J.R. McIntosh. 2006. The molecular architecture of axonemes revealed by cryoelectron tomography. *Science.* 313:944–948.

Oda, T., N. Hirokawa, and M. Kikkawa. 2007. Three-dimensional structures of the flagellar dynein–microtubule complex by cryoelectron microscopy. *J. Cell Biol.* 177:243–252.

Pettersen, E.F., T.D. Goddard, C.C. Huang, G.S. Couch, D.M. Greenblatt, E.C. Meng, and T.E. Ferrin. 2004. UCSF Chimera—a visualization system for exploratory research and analysis. *J. Comput. Chem.* 25:1605–1612.

Piperno, G., and Z. Ramanis. 1991. The proximal portion of *Chlamydomonas* flagella contains a distinct set of inner dynein arms. *J. Cell Biol.* 112:701–709.

Sale, W.S. 1986. The axonemal axis and Ca2+-induced asymmetry of active microtubule sliding in sea urchin sperm tails. *J. Cell Biol.* 102:2042–2052.

Satir, P. 1989. The role of axonemal components in ciliary motility. *Comp. Biochem. Physiol. Comp. Physiol.* 94:351–357.

Sui, H., and K.H. Downing. 2006. Molecular architecture of axonemal microtubule doublets revealed by cryo-electron tomography. *Nature.* 442:475–478.

Summers, K.E., and I.R. Gibbons. 1971. Adenosine triphosphate-induced sliding of tubules in trypsin-treated flagella of sea-urchin sperm. *Proc. Natl. Acad. Sci. USA.* 68:3092–3096.

Summers, K.E., and I.R. Gibbons. 1973. Effects of trypsin digestion on flagellar structures and their relationship to motility. *J. Cell Biol.* 58:618–629.

Wakabayashi, K., S. Takada, G.B. Witman, and R. Kamiya. 2001. Transport and arrangement of the outer-dynein-arm docking complex in the flagella of *Chlamydomonas* mutants that lack outer dynein arms. *Cell Motil. Cytoskeleton.* 48:277–286.

Wargo, M.J., and E.F. Smith. 2003. Asymmetry of the central apparatus defines the location of active microtubule sliding in *Chlamydomonas* flagella. *Proc. Natl. Acad. Sci. USA.* 100:137–142.

Witman, G.B. 1986. Isolation of *Chlamydomonas* flagella and flagellar axonemes. *Methods Enzymol.* 134:280–290.

Witman, G.B., K. Carlson, J. Berliner, and J.L. Rosenbaum. 1972. *Chlamydomonas* flagella: I. Isolation and electrophoretic analysis of microtubules, matrix, membranes, and mastigonemes. *J. Cell Biol.* 54:507–539.

Yagi, T., I. Minoura, A. Fujiwara, R. Saito, T. Yasunaga, M. Hirono, and R. Kamiya. 2005. An axonemal dynein particularly important for flagellar movement at high viscosity. Implications from a new *Chlamydomonas* mutant deficient in the dynein heavy chain gene DHC9. *J. Biol. Chem.* 280:41412–41420.

Yagi, T., K. Uematsu, Z. Liu, and R. Kamiya. 2009. Identification of dyneins that localize exclusively to the proximal portion of *Chlamydomonas* flagella. *J. Cell Sci.* 122:1306–1314.

Yoshimura, A., I. Nakano, and C. Shingyoji. 2007. Inhibition by ATP and activation by ADP in the regulation of flagellar movement in sea urchin sperm. *Cell Motil. Cytoskeleton.* 64:777–793.